AGU PUBLICATIONS

JGR

Journal of Geophysical Research: Biogeosciences

RESEARCH ARTICLE
10.1002/2017JG004336

Key Points:
- Interannual variability in tidal salt marsh NEE was explained by variation in rainfall and salinity
- A significant but small difference was determined between contemporary NEE and decadal burial rates
- Tidal losses may be a relatively small feature of the C budget in infrequently flooded high marshes

Correspondence to:
I. Forbrich,
iforbrich@mbl.edu

Citation:
Forbrich, I., Giblin, A. E., & Hopkinson, C. S. (2018). Constraining marsh carbon budgets using long-term C burial and contemporary atmospheric CO_2 fluxes. *Journal of Geophysical Research: Biogeosciences*, *123*, 867–878. https://doi.org/10.1002/2017JG004336

Received 29 NOV 2017
Accepted 31 JAN 2018
Accepted article online 6 FEB 2018
Published online 11 MAR 2018

Constraining Marsh Carbon Budgets Using Long-Term C Burial and Contemporary Atmospheric CO_2 Fluxes

I. Forbrich[1], A. E. Giblin[1], and C. S. Hopkinson[2]

[1]Marine Biological Laboratory, Woods Hole, MA, USA, [2]Department of Marine Sciences, University of Georgia, Athens, GA, USA

Abstract Salt marshes are sinks for atmospheric carbon dioxide that respond to environmental changes related to sea level rise and climate. Here we assess how climatic variations affect marsh-atmosphere exchange of carbon dioxide in the short term and compare it to long-term burial rates based on radiometric dating. The 5 years of atmospheric measurements show a strong interannual variation in atmospheric carbon exchange, varying from −104 to −233 g C m^{-2} a^{-1} with a mean of −179 ± 32 g C m^{-2} a^{-1}. Variation in these annual sums was best explained by differences in rainfall early in the growing season. In the two years with below average rainfall in June, both net uptake and Normalized Difference Vegetation Index were less than in the other three years. Measurements in 2016 and 2017 suggest that the mechanism behind this variability may be rainfall decreasing soil salinity which has been shown to strongly control productivity. The net ecosystem carbon balance was determined as burial rate from four sediment cores using radiometric dating and was lower than the net uptake measured by eddy covariance (mean: 110 ± 13 g C m^{-2} a^{-1}). The difference between these estimates was significant and may be because the atmospheric measurements do not capture lateral carbon fluxes due to tidal exchange. Overall, it was smaller than values reported in the literature for lateral fluxes and highlights the importance of investigating lateral C fluxes in future studies.

1. Introduction

Salt marshes have long been recognized for their critical role in processing and storing material passing between terrestrial ecosystems and the ocean. The accumulation of terrestrial sediments and soil organic matter are important mechanisms contributing to the development and maintenance of tidal wetlands relative to sea level rise (Morris et al., 2002; Redfield, 1965). Burial of organic matter and carbon (C) in sediments makes them strong sinks of atmospheric carbon dioxide (CO_2) (Chmura et al., 2003; Hopkinson et al., 2012; Mcleod et al., 2011). This C burial rate can be determined as average accumulation rates over the lifetime of key radioisotopes, for example, 50 to 100 years based on radiometric dating using ^{137}Cs and ^{210}Pb (Chmura et al., 2003; Mcleod et al., 2011). However, the sources of organic C burial, the relative contribution of in situ plant production, and the controls on burial are highly uncertain in wetland-dominated coastal system (Bauer et al., 2013). This is mostly due to a lack of large-scale measures of relevant fluxes over varying environmental conditions. In terrestrial systems, the eddy covariance method (Baldocchi et al., 1988) has been used to study the net ecosystem exchange (NEE) of carbon dioxide (CO_2) and its drivers at various scales (i.e., hourly to years). However, unlike in terrestrial systems, NEE in tidal wetlands may not fully represent net C accumulation, as considerable amounts of organic and inorganic forms of C are exchanged laterally with estuarine waters (Cai, 2011; Chapin et al., 2006; Wang et al., 2016, 2017). Nevertheless, NEE does have the potential to constrain lateral C fluxes. The difference between NEE measurements and burial rates allows to estimate the mass loss of C that is not exchanged with the atmosphere (e.g., Troxler et al., 2013).

Long-term annual measures of aboveground productivity reveal substantial variation from year to year (Morris & Haskin, 1990; Morris et al., 2013). This variation in marsh biomass production is most often explained by variation in drivers that affect soil salinity levels, such as anomalies in mean sea level, freshwater discharge, and rainfall (Hanson et al., 2016; Morris, 2000; Morris et al., 2002; Wieski & Pennings, 2014). Generally, high soil salinity levels reduce biomass production, for example, via inhibition of nutrient uptake (Morris, 1984) and/or CO_2 uptake via stomatal closure (Hwang & Morris, 1994). In contrast to variations in net biomass production, we know little about annual variations in marsh gross primary production (GPP), ecosystem respiration (R_{eco}), and NEE or the role of salinity variation as their drivers. Here we conducted eddy covariance measurements

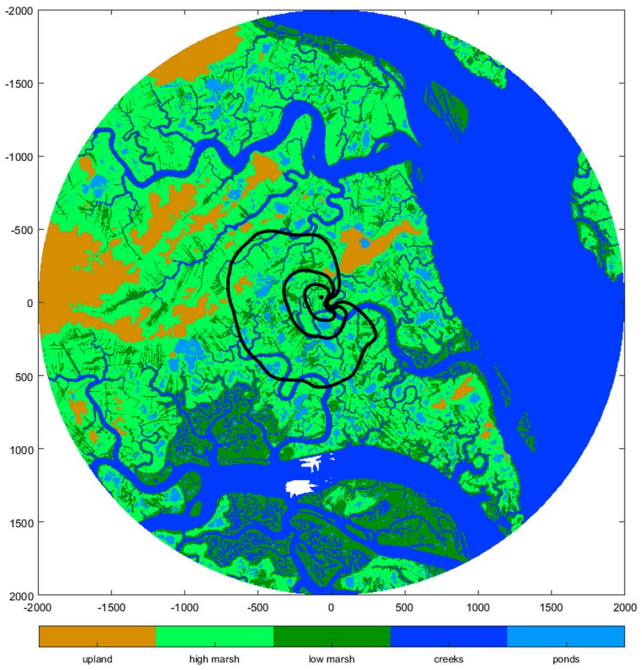

Figure 1. Land cover map of study site with footprint climatology (FFP v. 2.1) for all valid flux measurements in 2013. Coordinates are in meters, and the center point is the flux tower location. Radius is 2,000 m. Shown are the maximum of the footprint function and the 30%, 60%, and 90% footprint contribution. Land cover types are defined by elevation thresholds (in NAVD88) in a digital elevation model: upland (≥1.8 m), marsh (0.6–1.8 m), and creek (≤0.6 m). Ponds were digitized from 2005 imagery (Millette et al., 2010).

of CO_2 exchange for 5 years in a New England salt marsh and determined the long-term burial rate of organic carbon. We address the following questions: (1) What is the interannual variability in NEE and how does it relate to variation in climate? and (2) How does contemporary NEE differ from the long-term C burial rate?

2. Materials and Methods

2.1. Site Description

Carbon cycling processes were examined in a tidal salt marsh in the Plum Island Sound estuary in northeastern Massachusetts, USA. Tides are semidiurnal with an average range of 2.9 m and a spring-neap range of 2.6–4.0 m. The study site, as most of the marsh, is dominated by high marsh (elevation > 1.3 m in North American Vertical Datum of 1988 (NAVD88)), which is only inundated during biweekly spring tides and storms. Vegetation on the dominant high marsh platform is composed of *Spartina patens* and *Distichilis spicata* in well-drained areas with stunted *Spartina alterniflora* occurring in areas with limited drainage. Low marsh areas and creek banks make up less than 20% of the area and are predominantly vegetated by *Spartina alterniflora*. Ponds occur at both higher and lower elevations (Millette et al., 2010) and are dynamic features in the landscape (Wilson et al., 2014). The average habitat composition of the area contributing to the flux measurements is 1% upland, 9% ponds, 9% creeks, and 81% vegetated marsh (Figure 1).

2.2. Eddy Covariance and Meteorological Measurements

NEE was measured using the eddy covariance technique for 5 years beginning in 2013. To be able to measure continuous year-round fluxes, the flux tower was established on a small rocky upland outcrop within the high marsh, which protected it from winter ice damage. Wind velocity was measured by a 3-D sonic anemometer (CSAT-3A) mounted 14 m above the marsh surface. The relatively high measurement height was chosen in order to minimize the influence of the rock and shrub vegetation on the turbulence.

Sample air was drawn from the central point of the anemometer and drawn through a 60 cm long tube to an infrared gas analyzer (CPEC200). Pump flow rate was 7 L/min. Turbulent measurements were recorded with a frequency of 10 Hz. Air temperature and relative humidity (Campbell Scientific HC2S3) were monitored at the same height as the anemometer.

From May to end of October, a separate meteorological station was set up on the high marsh to record additional radiation data. A four-component net radiometer (Hukseflux NR01) was mounted 1.5 m above the high marsh surface. At the same height, two sensors (LI190SB) monitored incoming and reflected photosynthetically active radiation (PAR) to estimate a broadband Normalized Difference Vegetation Index (NDVI) according to Wilson and Meyers (2007). This index was used in our NEE model described below. Water table height was recorded with a pressure transducer (Campbell Scientific CS456). Soil temperature was recorded at depths of 2 cm, 6 cm, 10 cm, 20 cm, and 40 cm. In 2016 and 2017, measurements were expanded to include specific conductivity and temperature of surface well water on the high marsh (model 600R water quality sampling sonde, YSI Inc.) as described in Barr et al. (2010).

In the nongrowing season (November–April), the meteorological station was moved to a protected site close to the Plum Island Long-Term Ecological Research field station to record incoming and reflected radiation, albedo, and PAR as well as water table height. All meteorological data were recorded in 10 min intervals.

2.3. Eddy Covariance Data Processing

2.3.1. Flux Calculation and Quality Control

Atmospheric turbulent fluxes were calculated as covariance between vertical wind speed and dry mixing ratios (Novick et al., 2013). Signals were despiked, and two coordinate rotations were performed on the wind components. The time lag between wind and CO_2 mixing ratio measurements was determined within a set window between 0.1 and 0.3 s and removed for each averaging interval of 30 min. For every 30 min period,

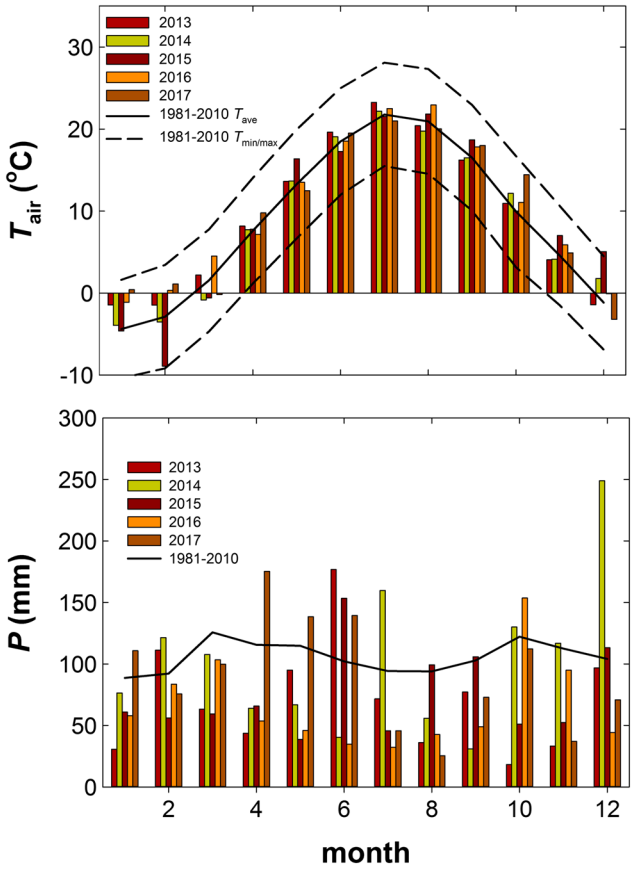

Figure 2. Air temperature (T_{air}, top) at the tower and precipitation (P, bottom) recorded at the recorded at the meteorological station run by the Long-Term Research Project meteorological station approximately 7 km away from the study site for the five study years. Thirty year averages for T_{air} and P (solid lines) and maxima and minima for T_{air} (dashed lines) are from a NOAA station in Haverhill, MA, approximately 20 km from the study site.

a factor for the correction of the frequency attenuation of the flux was calculated according to Moore (1986) and applied to the flux. Fluxes were calculated using the Edire software (version 1.5.0.32, R. Clement, University of Edinburgh, UK).

The calculated fluxes were filtered for system malfunctioning and calibration periods, integral turbulence characteristics, stationarity, and wind direction (Foken et al., 2012). Outliers were filtered out using the approach described by Papale et al. (2006). Furthermore, we excluded data when (a) the footprint was not representative for the high marsh, that is, included large fractions of upland and large water bodies (0–115°, Figure 1) and (b) when the 80% footprint extended more than 2,000 m (see below and Figure 1). On average 48% of the observations were removed before filtering nighttime fluxes during low turbulent conditions.

The thresholds in friction velocity and their uncertainty were determined according to Papale et al. (2006) as implemented in REddyProc 0.8-2 (Department for Biogeochemical Integration, 2016).

2.3.2. NEE Gap-Filling, Partitioning, and Uncertainty

Processes that have short-term effects on CO_2 fluxes from marsh sediments and plants, such as temperature, radiation, and tidal inundation, need to be considered in NEE modeling. We have not observed such short-term effects in the nongrowing season, and thus we used the mean diurnal variation method (Falge et al., 2001) to fill gaps in the fluxes from November to April (using 10 day windows). During the growing season, however, we have used an adjusted PLIRTLE model (using 8 day windows) (Forbrich & Giblin, 2015), to partition the growing season fluxes (May–October) into GPP and ecosystem respiration (R_{eco}). Following the approach developed in Forbrich and Giblin (2015), we can account for the reduction of GPP and R_{eco} during inundation of plant tissues by using the simultaneous reduction in NDVI which mimics the decrease in soil and vegetation exposed to the atmosphere:

$$\mathrm{NEE} = \mathrm{GPP} + R_{\mathrm{eco}} \tag{1}$$

$$\mathrm{GPP} = \frac{P_{\max}}{k} \times \ln\left(\frac{P_{\max} + \alpha \times I}{P_{\max} + \alpha \times I \times \exp -k \times \mathrm{NDVI}}\right) \tag{2}$$

$$R = R_{\mathrm{ref}} \times \mathrm{NDVI} \times \exp\left(E_0 \times \left(\frac{1}{T_{\mathrm{ref}} - T_0} - \frac{1}{T - T_0}\right)\right) \tag{3}$$

where NDVI is the gap-filled time series of NDVI determined on site (Forbrich & Giblin, 2015), I is PAR (μmol m^{-2} s^{-1}), T is air temperature (°C), T_{ref} is the reference temperature set to 15°C, and T_0 is −46.02°C). P_{max} is the light-saturated photosynthetic rate (μmol m^2 s^1), k is the Beer's light extinction coefficient (fixed to 0.5), and α is the initial slope of the light response curve (μmol CO_2 μmol photons^{-1}). R_{ref} is the temperature-independent level of respiration (μmol CO_2 m^{-2} s^{-1}), while E_0 is a short-term temperature sensitivity parameter (μmol CO_2 m^{-2} s^{-1}) (Reichstein et al., 2005).

To estimate the effect of random measurement uncertainty and gap-filling uncertainty on the integrated net and gross fluxes, we used a Monte Carlo approach based on Richardson and Hollinger (2007). We estimated the random measurement uncertainty following Finkelstein and Sims (2001). We then created 100 flux data sets by adding normally distributed random noise to the observations and their individual error. For each run the gap-filling procedure described above was implemented. We then calculated the mean of the integrated fluxes from the 100 runs and its 95% confidence interval.

2.3.3. Land Cover Map and Footprint Modeling

We distinguished between four different land cover types: forested upland, vegetated marsh, marsh creeks, and marsh ponds. We use a digital elevation model (Millette et al., 2010) to separate the first three based on elevation thresholds (Figure 1). Ponds were digitized from 2005 imagery (Millette et al., 2010).

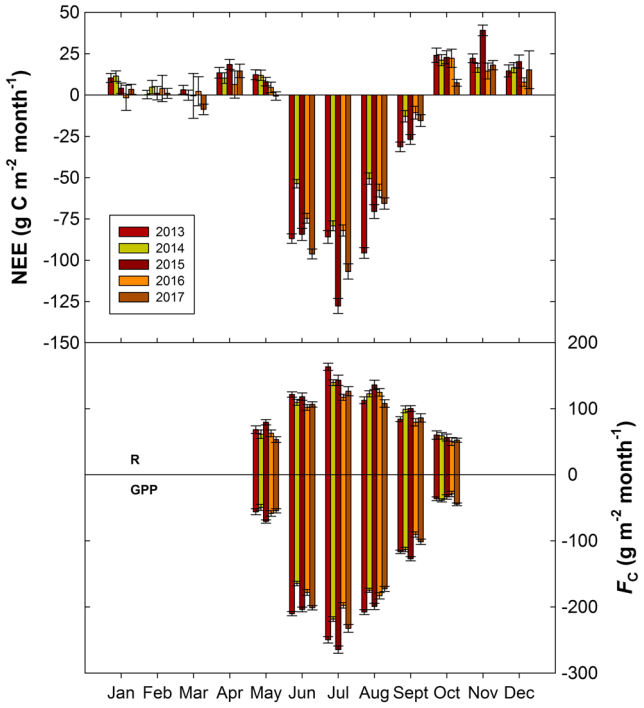

Figure 3. Average monthly budgets for net ecosystem exchange (NEE) (top) and gross primary production (GPP) and R_{eco} (bottom). Values are u_* corrected. NEE displays a pronounced seasonality with net release (positive fluxes) from October to May and strong net uptake (negative fluxes) from June to September when GPP dominates (bottom).

We ran the 2-D footprint parametrization (FFP) by Kljun et al. (2015), which is based on the Langrangian particle dispersion model of Kljun et al. (2002) and suitable for convective to stable boundary layer conditions. It was run with inputs derived from measurements of measurement height, wind speed, Obukhov length (which characterizes the relative contributions from buoyant and shear production to turbulent kinetic energy), u_*, standard deviation of lateral velocity fluctuations, and wind direction to calculate 30 min 80% footprints. Values for roughness length were set to 0.015 to account for the short marsh plant canopies and adjusted for snow cover (z_0 = 0.002 m) and flooding (z_0 = 0.001 m). The boundary layer heights were estimated according to Kljun et al. (2015). The land cover composition of the 30 min footprints was determined overlaying the footprints with each land cover map (Figure 1).

2.3.4. Controls on Interannual Variability in NEE

We studied the controls on interannual variability in annual C uptake using the approach described by Zscheischler et al. (2016). It identifies days with high fluxes ("most active days") that best explain the variation in annual C fluxes and analyzes their environmental drivers. Most active days were defined as days when fluxes crossed the 85th percentile of the aggregated flux distribution of all years.

We analyzed whether most active days could be separated from the remaining days using a principal component analysis (PCA) of environmental drivers. We used the same drivers as Zscheischler et al. (2016): *day of the year*, *temperature*, *PAR*, *vapor pressure deficit (VPD)*, and *cumulative rainfall of the previous 30 days*. We also estimated the growing season length as a possible alternative to most active days. Beginning and ending of the growing season were defined as the point in time when the smoothed daily GPP value crossed a threshold set to 10% of the 99th percentile of summer GPP values across all years.

2.4. Moderate Resolution Imaging Spectroradiometer NDVI

To monitor vegetation dynamics, we used satellite data from the Moderate Resolution Imaging Spectroradiometer (MODIS) that have been filtered for tidal flooding conditions (O'Connell et al., 2017). These images were used to generate an NDVI time series composite for 8 day windows. We estimated parameters related to phenology using a double logistic model (Beck et al., 2006) after filtering for outliers. NDVI was modeled as a function of time (t) using six parameters: the winter NDVI (wNDVI); the maximum NDVI (mNDVI) during the growing year; two inflection points, one as the curve rises (S) and one as it drops (A); and the rate of increase or decrease (mS and mA) of the curve at the inflection points.

$$\mathrm{NDVI}(t) = \mathrm{wNDVI} + (\mathrm{mNDVI} - \mathrm{wNDVI}) \times \left(\frac{1}{1 + \exp(-\mathrm{mS} \times (t - S))} + \frac{1}{1 + \exp(\mathrm{mA} \times (t - A))} - 1 \right) \quad (4)$$

2.5. Peat Core C Content, Radiometric Dating, and Rates of C Burial

In October 2014, four 40 cm deep cores were taken on the high marsh platform within 20–40 m of the flux tower. Two were taken in stunted *S. alterniflora*, and two were taken in *S. patens*. Cores were taken to the lab and stored at 4°C before further analysis.

Cores were sectioned in 2 cm layers, which were subsequently dried. Bulk density was determined on the section, which was subsequently ground. Subsamples for CHN analysis (Thermo Scientific Flash 2000 NC Soil Analyzer) were first hydrated and then fumed with HCl to remove carbonates. The core sections were dated based on profiles of ^{137}Cs and ^{210}Pb. We used a pure germanium gamma spectrometer (Canberra, GCW3023) to measure gamma emissions of ^{210}Pb (46 keV), ^{137}Cs (661.62 keV), ^{214}Pb (352 keV), and ^{214}Bi (609.32 kev). ^{214}Pb and ^{214}Bi were used to determine unsupported ^{210}Pb, as a measure of ^{226}Ra. Subsamples for radiochemical analysis were sealed for at least 21 days to ensure equilibrium between ^{226}Ra and ^{210}Pb before counting.

Table 1
Growing Season Length (GSL) and Most Active Days (MAD) for NEE, GPP, and R_{eco} (All in Days)

Year	GSL	NEE	GPP	R_{eco}
2013	168	64	45	36
2014	173	45	18	33
2015	162	66	43	54
2016	160	55	13	12
2017	177	62	28	12
n_{all}	—	1,826	920	920
85th percentile	—	2.4	7.5	4.4

Note. MAD were determined as flux values above the 85th percentile of the aggregated flux distribution of all years (n_{all} = 1,826) or all growing seasons (n_{all} = 920). These thresholds are given in g C m^{-2} a^{-1}. NEE = net ecosystem exchange; GPP = gross primary production.

^{137}Cs is a product of bomb-derived fallout with an expected peak indicating 1963. ^{210}Pb activity depends on two sources, supported activity from radioactive decay of the natural ^{226}Ra occurring in the sediments and the unsupported ^{210}Pb activity from atmospheric fallout. The age of sediments (t) can be determined with $C_{xs}(t)$ as the measured excess ^{210}Pb activity and $C_{xs}(0)$, the unknown initial activity, from equation

$$C_{xs}(t) = C_{xs}(0) \times \exp(-\lambda \times t) \quad (5)$$

provided that the value for the initial activity ($C_{xs}(0)$), which depends on the rate of atmospheric fallout, can be estimated (Appleby, 2008). Here we assume a constant initial activity and a constant sedimentation rate (CIC model; Krishnaswamy et al., 1971). Mass accumulation rates were determined based on mass depth. We calculated the ^{137}Cs-derived accumulation rates by dividing the mass depth of the ^{137}Cs activity peak by 51 (the number of years between sampling and 1963). Using the CIC model, we calculated a single mass accumulation rate from a plot of the natural log of the excess activity with mass depth. Burial rates are based on each mass accumulation rate times the average C concentration below the rooting zone (i.e., of the lowest 10 cm of each core; 11–16%; section 3.4.1).

Accretion rates were determined as described above, but using soil depth instead of mass depth. Finally, to evaluate the dating, we compare the age derived from the CIC model with the ^{137}Cs peak.

$$t_{CIC} = \frac{z_i}{\text{accretion rate}} \quad (6)$$

with z_i as soil depth.

2.6. Comparison of NEE and Burial Rates

We tested whether the difference between the mean annual NEE of the four years and the mean of the burial rates was significantly different from 0. To do so, we used a bootstrap analysis to determine the 95% confidence interval of the difference. This analysis repeatedly sampled both data sets with substitution 100 times to recalculate the mean difference and its confidence interval.

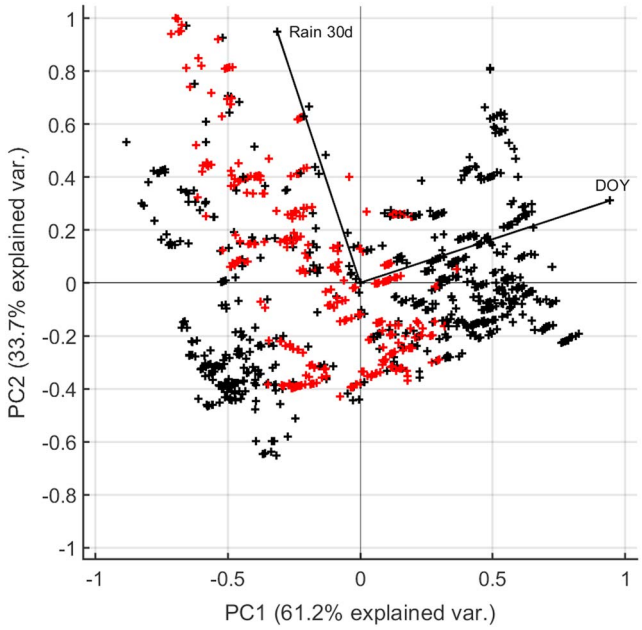

Figure 4. Principal component analysis for environmental drivers from May to October, projection on the first two principal components (PC). Most active days of net ecosystem exchange are in red, others in black. DOY = day of year, Rain 30d = cumulative rainfall over the previous 30 days.

3. Results

3.1. Meteorology

Annual average temperatures at the marsh site between 2013 and 2017 were higher than the long-term average of 8.7°C (NOAA, Haverhill, MA, USA, USC00193505). Annual precipitation over the 5 year period was lower than the long-term average of 1269mm (1981–2010) with marked seasonal differences between the years. In the long term, rainfall is fairly evenly distributed over the year with two smaller peaks in spring and fall (Figure 2). Summer rainfall varied markedly over the five years, especially in June. In 2013, 2015, and 2017, monthly rainfall was above average; in the other two years it was below average. In 2016, measured rainfall was below average throughout the growing season (Figure 2).

3.2. CO_2 Fluxes

3.2.1. Net Ecosystem Exchange of CO_2

Net CO_2 fluxes showed a pronounced seasonality in all years. The marsh acts as a net source to the atmosphere from October to May and as a substantial net sink from June to September (Figure 3). Lowest fluxes occur in February and March when the soil temperature is close to freezing (data not shown). In all years, the marsh was a strong net carbon sink but the strength of this sink varied considerably. Annual net uptake was similar

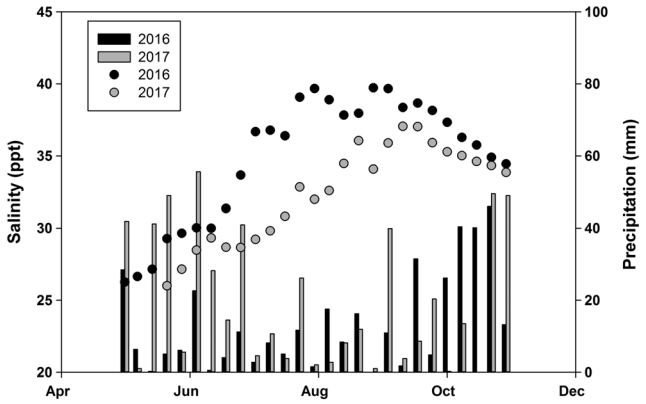

Figure 5. Weekly rainfall sums and averages of porewater salinity measured on the high marsh in 2016 and 2017.

in 2013 (-199 ± 12 g C m^{-2} a^{-1}), 2015 (-196 ± 17.1 g C m^{-2} a^{-1}), and 2017 (-233 ± 17 g C m^{-2} a^{-1}) but lower in 2014 (-104 ± 11 g C m^{-2} a^{-1}) and in 2016 (-165 ± 13 g C m^{-2} a^{-1}).

3.2.2. CO_2 Flux Components

The component fluxes GPP and R_{eco} showed strong seasonal trends in all five years (Figure 3). In 2013, 2015, and 2017, GPP in June and July was greater than in the other two years. During the period May–October, GPP varied from -807 ± 10 (2017) and -877 ± 10 (2013) to -900 ± 10 g C m^{-2} (2015) compared to -759 ± 9 and -737 ± 13 g C m^{-2} for 2014 and 2016. Monthly R_{eco} did not show this systematic variability between years. Growing season R_{eco} tended to be higher in 2013 and 2015 (606 ± 12.8 and 643 ± 16.6 g C m^{-2}, respectively) than in 2014 and 2016 (581 ± 11 and 539 ± 14 g C m^{-2}) but not in 2017 (532 ± 13 g C m^{-2}).

3.2.3. Controls on Interannual Variability in NEE

We found that the number of most active days per year explained variation in annual C fluxes better than the length of the growing season (Zscheischler et al., 2016): The latter varied little between the years, ranging from 160 days (2016) to 177 days (2017), and did not vary with annual net uptake. Contrasting this, the number of most active days for NEE varied between years and higher numbers occurred in 2013, 2015, and 2017 (Table 1). Meanwhile, the seasonal distribution of most active days did not vary between years (data not shown).

In our PCA analysis we found two main drivers linked to the observed variability. Most variation within the selected climate drivers described above occurs seasonally and thus were separated along the direction of day of year (DOY) within the PCA. This first principal component explained 61.2% of the variance; the second component was directed toward "cumulative rainfall in prior 30 days" and explained 33.7% (Figure 4). Most active days were generally separated along the second principal component, indicating a positive effect of rainfall on annual NEE (Figure 4). The most likely way in which rainfall impacts variability in NEE is through altering soil salinity. Measurements taken in 2016 (dry) and 2017 (wet) show a marked divergence of salinity in June and July which corresponded to the large differences in early season rainfall (Figure 5).

3.3. MODIS NDVI

NDVI started to increase at the beginning of May and started to decrease in September during all five years (Figure 6). The fitted double logistic curve described this pattern. Fitting parameters did not significantly differ between years except the one describing the early inflection point (Table 2). It is significantly earlier in 2013, 2015, and 2017 than in the other two years, describing an earlier increase in NDVI which results in a higher peak NDVI in these three years (Figure 6).

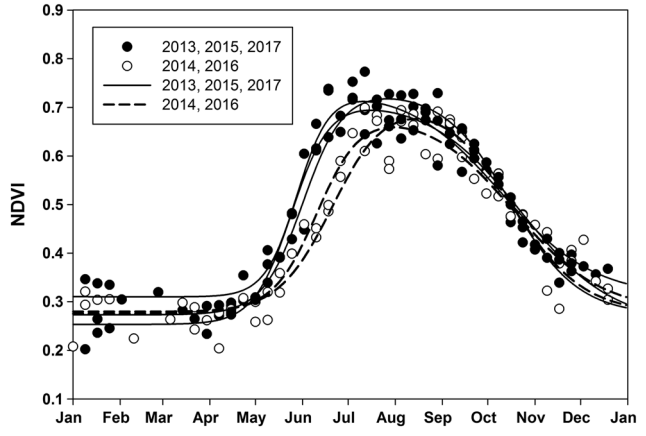

Figure 6. Moderate Resolution Imaging Spectroradiometer Normalized Difference Vegetation Index (NDVI), filtered for tidal inundation according to O'Connell et al. (2017) and double logistic model fit (Table 2). NDVI in 2013, 2015, and 2017 increases earlier than in the other two years.

3.4. Sediment Core Analysis

3.4.1. Sediment Characteristics

Sediment bulk density did not show a consistent trend with depth in the four cores (Figure 7). The average of the upper 10 cm is 0.22 g cm^{-3} and of the lowest 10 cm is 0.25 g cm^{-3}. The carbon content in all four cores ranged from 8.8% to 23.9% and was generally higher in the top 25 cm than below. This corresponds to our observation that below that depth the root density is less than in the top soil. Average C content in the upper 10 cm was 16% carbon and 12.5% in the lowest 10 cm (core 1: 11%, core 2: 12%, core 3: 16%, and core 4: 11%). These values fall well in the range of a recent synthesis (Morris et al., 2016).

3.4.2. Mass Accumulation and Burial Rates

Excess ^{210}Pb activities decreased exponentially with (mass) depth in all four cores (Figure 8). The ^{137}Cs peak occurred at slightly different depths in each core, ranging from 16 cm to 25 cm. The age estimates for the two techniques agreed well, with the exception of core 3 (Table 3). Its ^{210}Pb depth profile was irregular which resulted in an unreasonably young age estimate for the section with the 1963 ^{137}Cs peak. We thus excluded the ^{210}Pb data from core 3 from any further calculation.

Table 2
Fitting Parameters of Double Logistic Model (Beck et al., 2006)

Year	*n*	wNDVI	mNDVI	mS	S	mA	A
2013	32	0.27 (±0.01)	0.74 (±0.01)	0.08 (±0.01)	152 (±1)	0.05 (±0.0)	288 (±2)
2014	35	0.28 (±0.01)	0.69 (±0.02)	0.07 (±0.01)	161 (±2)	0.04 (±0.01)	294 (±4)
2015	34	0.25 (±0.01)	0.72 (±0.01)	0.08 (±0.01)	145 (±1)	0.03 (±0.01)	284 (±2)
2016	37	0.27 (±0.0)	0.74 (±0.04)	0.06 (±0.01)	172 (±3)	0.04 (±0.01)	294 (±5)
2017	33	0.31 (±0.0)	0.75 (±0.02)	0.09 (±0.01)	149 (±1)	0.03 (±0.01)	294 (±4)

Note. Values in parentheses indicate their 95% confidence interval. NDVI = Normalized Difference Vegetation Index; wNDVI = winter NDVI; mNDVI = maximum NDVI. S and A are inflection points of the curve, representing transition of growing season, and mS and mA the change of the curve.

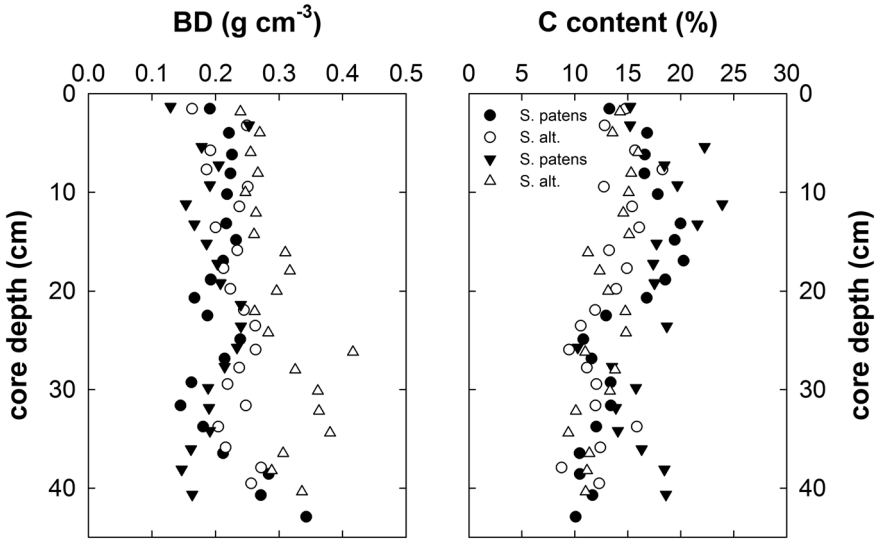

Figure 7. Depth profiles of bulk densities (BD, left) and carbon (C, right) content of all four cores.

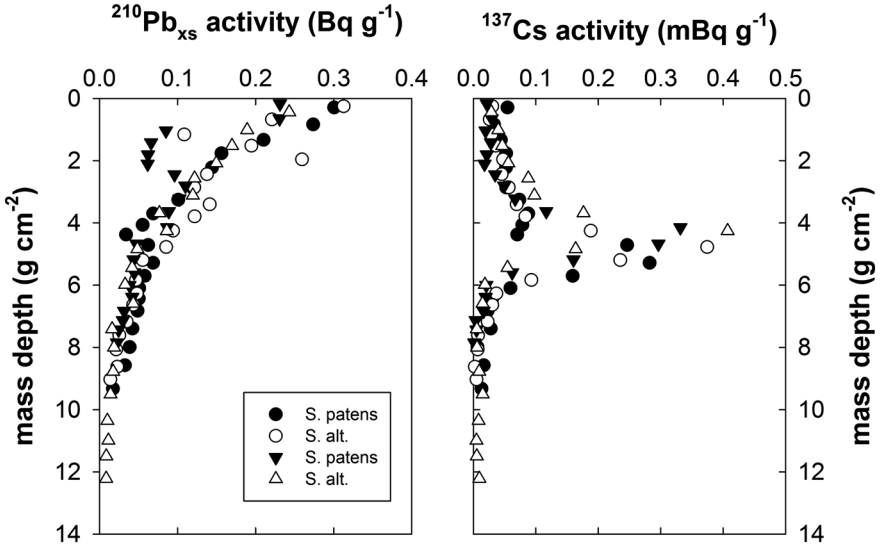

Figure 8. Profiles of radioisotope activities along mass depth. ^{137}Cs activities are uncorrected for counting efficiency.

Table 3
Dating Results for All Four Cores Taken in 2014

Core	Depth of ^{137}Cs peak (cm)	^{210}Pb age at ^{137}Cs peak (years)	Accretion rate (^{137}Cs) (cm a^{-1})	Accretion rate (^{210}Pb) (cm a^{-1})	Mass accumulation rate (^{137}Cs) (g m^2 a^{-1})	Mass accumulation rate (^{210}Pb) (g m^2 a^{-1})	C burial (^{137}Cs) (gC m^2 a^{-1})	C burial (^{210}Pb) (gC m^2 a^{-1})
1	25	52	0.49	0.48	1,036	1,012	114	111
2	22	56	0.43	0.39	936	918	112	110
3	21	42	0.42	—	813	—	130	—
4	16	50	0.32	0.32	843	998	93	110
Mean $\pm 2\sigma$					907 $\pm$ 201	976 $\pm$ 99	112 $\pm$ 15	110 $\pm$ 1

Note. The ^{137}Cs peak (depth in centimeters) is 51 years ago which should agree with the age determined from the CIC model using ^{210}Pb (age in years). Accretion rates (cm a^{-1} and mass accumulation rates (g m^2 a^{-1}) were determined from the (mass) depth of the ^{137}Cs peak or a fit of ^{210}Pb activities against depth or mass depth. C burial rates (in g C m^2 a^{-1}) were estimated using mass accumulation rates multiplied with average C content of the lowest 10 cm. Values are shown for single cores and means $\pm 2\sigma$.

Both accretion and mass accumulation rates agreed well between methods, with accretion rate estimates ranging from 0.32 cm a^{-1} to 0.49 cm a^{-1} (^{137}Cs) or 0.32 cm a^{-1} to 0.48 cm a^{-1} (^{210}Pb) (Table 3). Since there were no large variations in C density between cores, the average C burial rates agreed very well between the two methods as well: 112 $\pm$ 15 g C m^2 a^{-1} (^{137}Cs) and 110$\pm$ g C m^2 a^{-1} (^{210}Pb).

3.5. Comparison of NEE and Burial Rates

The average annual NEE over the five years was significantly greater than the burial rate by 69 g C m^2 a^{-1} (95% confidence interval 25 – 103 g C m^2 a^{-1}).

4. Discussion

4.1. Rainfall as Driver of Marsh Productivity

In the five years presented here, the magnitude of net CO_2 uptake between years can best be explained by the occurrence of high fluxes during the growing season rather than growing season length (Zscheischler et al., 2016). At this site, the growing season length is short and characterized by rapid growth in June (Morris et al., 2013). This strong seasonality is evident in all years, but higher fluxes are associated with high rainfall in the prior month, which at our site reflects lower soil salinity levels (Figure 5). Corresponding to high rainfall events, NDVI values are higher during summer months with more rainfall (2013, 2015, and 2017) compared to the other two years, indicating higher biomass production during these years. Similarly, Mo et al. (2017) found low NDVI values in June and July in *Spartina* marshes in Louisiana during drought years, when plant growth was inhibited. Rainfall, together with tidal inundation and evapotranspiration, controls soil salinity levels in salt marshes (e.g., Hughes et al., 2012), which regulates marsh productivity (Morris, 2000). For example, under anaerobic conditions, increased salinity inhibits ammonium uptake by *S. alterniflora* and *S. patens* (Bradley & Morris, 1991; Morris, 1984). A direct effect on photosynthesis in *S. alterniflora* occurs during increasing salinities via a reduction in stomatal conductance (Hwang & Morris, 1994). A comparison of soil salinity between 2016 and 2017 shows lower salinities in 2017 early in the growing season when rainfall was higher than in the previous year. This would have created favorable conditions for plant growth in a critical phase of plant development (Figure 6), explaining our observation of higher NDVI and GPP in summer 2017 and possibly in 2013 and 2015. The resulting higher NDVI in these years would indicate an increased capacity for light absorption by the marsh canopy and thereby increase GPP overall (Baldocchi et al., 2018). These observations support the finding that timing of rainfall is more important for plant growth than its magnitude in salt marshes (Chu et al., 2018; Hanson et al., 2016). For example, above average rainfall occurred in July 2014, which seems to have been too late in the growing season to have any positive effect on GPP. Similarly, Chu et al. (2018) find a positive effect of rainfall on NEE by decreasing soil salinity levels during the period of rapid growth but less or even negative effects in later parts of the season.

R_{eco} shows less annual variation than GPP, though it tends to be higher in more productive years. Conditions that increase GPP from one year to another are usually accompanied by a proportional but smaller increase in R_{eco} (Baldocchi et al., 2018). However, in some freshwater wetlands, an increase in R_{eco} has been observed during extended periods of low rainfall as a consequence of a lowered water table, which decreases productivity

if plants become water stressed and increases aerobic decomposition (Aurela et al., 2007; Helfter et al., 2015; Lund et al., 2012; Peichl et al., 2014). We did not observe this effect in the salt marsh described here, where regular tides prevent a prolonged lowering of the water table and peat oxidation.

At PIE, productivity of *S. alterniflora* growing at a lower elevation than at our site correlates positively with the mean high water (MHW) during the growing season, as tidal flushing helps regulate salinity as well as hypoxia in marsh porewaters (Morris et al., 2013). However, in higher elevation marshes dominated by *S. patens*, Morris et al. (2013) could not detect a similar correlation between productivity with MHW. This may in part be due to larger variability around biomass measurements of *S. patens* which forms dense carpets of stems. However, at higher elevation sites and especially in areas with limited drainage (i.e., the most salt stressed areas), rainfall rather than tidal inundation may be the dominant control on soil salinity in these interior marsh areas (Gross et al., 1990).

4.2. Marsh Carbon Storage

It is well established that salt marshes are strong sinks of organic carbon as long as they continuously gain elevation. This vertical growth isolates deeper soil layers from the input of labile carbon via roots and rhizomes (Morris & Bowden, 1986). The assumption as summarized by Morris et al. (2016) is that sediment volume within the rooting zone is influenced by loss of volume due to decomposition, erosion, and compaction and gains in volume due to the addition of roots, rhizomes, and surface deposition. Because only the refractory portion contributes to accretion and long-term C burial, the final volume is only achieved when the organic matter is stabilized, which is well below the rooting zone (Davis et al., 2015; Morris & Bowden, 1986). Therefore, in assessing burial rates from sediment cores, we have used the C content from below the rooting zone (Figure 7) as a proxy for this refractory portion of soil C and assume negligible further compaction. The resulting burial rates are in the range of estimates recently reviewed for New England by Drake et al. (2015) ranging from 74 to 257 g C m^{-2} a^{-1}. As the authors mention, the considerable variation is likely due to the differing sampling depths, varying bulk densities, and estimation techniques of C applied in each study. However, their estimated C accumulation rates for Plum Island marshes were similar to ours (87 (using ^{137}Cs) to 116 (using ^{210}Pb CIC) g C m^{-2} a^{-1}).

Conceptually, sediment C accumulation rates can be assumed to equal the net ecosystem carbon balance (NECB) budget, that is, the amount of C stored in the system. In tidal wetlands, NEE may exceed these burial rates because the marsh is known to export carbon to the estuary via porewater drainage and tidal flushing (Raymond & Hopkinson, 2003; Vallino et al., 2005). As expected, our measured NEE indicates a larger net C uptake than the burial rate, and this difference may be used as first-order estimate of lateral C export (Troxler et al., 2013). At our site this would suggest a bulk lateral export on the order of 69 g C m^{-2} a^{-1}. This is considerably less than the 400 g C m^{-2} a^{-1} estimated by Wang et al. (2016) for dissolved inorganic carbon (DIC) export alone.

One reason for the low estimate of C export may be the marsh and creek morphology of Plum Island. The hot spot for this exchange is the marsh interface along the creeks (Gardner & Gaines, 2008). Marshes at Plum Island are relatively high in elevation and flooded only during spring tides. Most of the flux footprint represents the marsh interior (Figure 1), which is characterized by limited drainage and flooding frequency. Therefore, the creekbanks do not have a large influence on the overall NEE measurements. Another issue may be the different fate of the two main dissolved C compounds: In the creekbank, porewater concentration can be elevated by 0.7 mM and 4.7 mM for dissolved organic carbon (DOC) and DIC, respectively (Raymond & Hopkinson, 2003). Prior estimates suggest that export of DOC alone can support a large fraction of estuarine respiration (Vallino et al., 2005). Since DIC porewater concentrations are higher than DOC concentrations, the DIC flux is likely larger than the DOC flux (Wang et al., 2016). The fate of this marsh-derived DIC is a critical question for resolving marsh-estuarine GPP and *R* estimates (Wang et al., 2017). Depending on pH values, DIC may be exported as alkalinity dissolved in water and/or as a gas which may be lost to the atmosphere. Raymond and Hopkinson (2003) estimated that about 50% of the porewater DIC was gaseous CO_2. It seems likely that this emission is captured by the atmospheric flux measurements. However, considering the small spatial extent of aquatic systems compared to vegetated marsh at our site (Figure 1), the atmospheric net flux is dominated by processes in the vegetated marsh (Pelletier et al., 2015). To further resolve these pathways, atmospheric measurements from vegetated and aquatic systems need to be combined with hydrological ones (Kearney et al., 2017; Wang et al., 2016).

An additional reason why the NEE from our flux tower may not match burial rates is the different temporal scales of the two approaches. The dating using ^{210}Pb allows us to calculate a mean accumulation rate over approximately 100 years. During this time period, sea level rise has accelerated and changes in sediment deposition and productivity may have occurred that all together increased accretion and burial rates (Hill & Anisfeld, 2015). The fairly deep depth of the rooting zone at our site does not allow us to accurately determine changes in accumulation rates over the last 30 years to test this hypothesis. However, there is some reason to suspect that the last few years could have been a time of enhanced marsh productivity. At Plum Island, *S. alterniflora* marshes are at an elevation that is above their optimum growth elevation (Morris et al., 2013). Because of their high elevation, aboveground productivity of *S. alterniflora* correlates positively with MHW during the growing season, an indication of increased tidal flushing that alleviates soil salinity and sulfide levels (Morris et al., 2013). MHW does vary between years with changes in the tidal amplitude, which are driven by astronomical forcing components such as the 18.6 lunar nodal cycle. For example, Morris et al. (2013) reported an increase of 14 cm in tidal amplitude from 2007 to 2011, during the rising phase of the current nodal cycle. It is around the peak (in 2015) of this phase that we started with our atmospheric measurements. Thus, we possibly overestimate the "mean" marsh net CO_2 uptake because of the short duration and the timing of our measurement period relative to the lunar nodal cycle. However, long-term climate records at Haverhill indicate that roughly a third of all years since 1950 (20 out of 67 years) are characterized by below-average rainfall in June. This is a somewhat smaller proportion than in our sampling period, where 40% of the years indicate below average rainfall. This would suggest that our mean NEE is actually underestimated—as would be the difference between NEE and burial. In either case, longer flux measurements are necessary to adequately sample long-term drivers (Chu et al., 2017). This is true with regard to temperature changes as well. The 5 years of measurements reported here are all above the long-term average, but at this point it is not known whether C accumulation will increase due to more biomass production or decrease due to increased decomposition.

5. Conclusions

We studied salt marsh C storage using 5 years of atmospheric measurements of CO_2 exchange and by estimating long-term C accumulation rates in sediment cores. The atmospheric flux measurements showed that the seasonality in fluxes was very similar between the five years. However, the flux magnitude in the growing season differed and decreased with rainfall and NDVI in 2014 and 2016. Rainfall and other hydrological variables may serve to regulate plant growth and NEE through soil salinity (as seen in our 2016 and 2017 data). Overall, the mean in net uptake over 5 years was 179 $\pm$ 32 g C m^{-2} a^{-1} and significantly larger than carbon storage measured in sediment cores (110 $\pm$ 13 g C m^{-2} a^{-1}). This difference may be attributed to missing lateral C fluxes in the aquatic phase and/or to changes in marsh productivity over time and the different time scales captured by our two measures. The first explanation suggests that atmospheric measurements of CO_2 exchange need to be coupled with measurements of lateral exchange of both DOC and DIC to determine the contemporary NECB in tidal wetlands. The second explanation argues for long-term data sets of CO_2 exchange that allow an assessment on the appropriate time scales.

Acknowledgments
Data used in this work have been assigned a digital object identifier and are accessible through the LTER Network Information System Data Portal (see Giblin & Forbrich, 2018a–2018f). We would like to thank Sam Kelsey, Sam Bond, Hap Garritt, and Jimmy Nelson (all MBL) for help during the installation of the flux tower. Sam Kelsey did the CHN analysis of the sediment samples. Jane Tucker (MBL) did the counting. Jessica O'Connell (UGA) provided the tide-filtered MODIS NDVI data. The Parker River National Wildlife Refuge and David F. Jaquith (Rowley) allowed us access to the location of tower and the winter met station, respectively. We would like to thank J. Matthes (Wellesley) and two anonymous reviewers for their comments on earlier drafts. PIE LTER is funded by NSF grants OCE-1637630 and OCE-1238212. Additional funding came from NSF 1426308 (Coastal SEES).

References

Appleby, P. (2008). Three decades of dating recent sediments by fallout radionuclides: A review. *The Holocene*, *18*(1), 83–93.
Aurela, M., Riutta, T., Laurila, T., Tuovinen, J.-P., Vesala, T., Tuittila, E.-S., et al. (2007). CO_2 exchange of a sedge fen in southern Finland—The impact of a drought period. *Tellus B*, *59*(5), 826–837.
Baldocchi, D., Chu, H., & Reichstein, M. (2018). Inter-annual variability of net and gross ecosystem carbon fluxes: A review. *Agricultural and Forest Meteorology*, *249*, 520–533.
Baldocchi, D. D., Hincks, B. B., & Meyers, T. P. (1988). Measuring biosphere-atmosphere exchanges of biologically related gases with micrometeorological methods. *Ecology*, *69*(5), 1331–1340.
Barr, J. G., Engel, V., Fuentes, J. D., Zieman, J. C., O'Halloran, T. L., Smith, T. J., & Anderson, G. H. (2010). Controls on mangrove forest-atmosphere carbon dioxide exchanges in western Everglades National park. *Journal of Geophysical Research*, *115*, G02020. https://doi.org/10.1029/2009JG001186
Bauer, J. E., Cai, W.-J., Raymond, P. A., Bianchi, T. S., Hopkinson, C. S., & Regnier, P. A. G. (2013). The changing carbon cycle of the coastal ocean. *Nature*, *504*(7478), 61–70.
Beck, P. S., Atzberger, C., Hogda, K. A., Johansen, B., & Skidmore, A. K. (2006). Improved monitoring of vegetation dynamics at very high latitudes: A new method using MODIS NDVI. *Remote Sensing of Environment*, *100*(3), 321–334.
Bradley, P. M., & Morris, J. T. (1991). The influence of salinity on the kinetics of NH_4 uptake in Spartina alterniflora. *Oecologia*, *85*(3), 375–380.
Cai, W.-J. (2011). Estuarine and coastal ocean carbon paradox: CO_2 sinks or sites of terrestrial carbon incineration? *Annual Review of Marine Science*, *3*(1), 123–145.
Chapin, F. S., Woodwell, G. M., Randerson, J. T., Rastetter, E. B., Lovett, G. M., Baldocchi, D. D., et al. (2006). Reconciling carbon-cycle concepts, terminology, and methods. *Ecosystems*, *9*(7), 1041–1050.

Chmura, G. L., Anisfeld, S. C., Cahoon, D. R., & Lynch, J. C. (2003). Global carbon sequestration in tidal, saline wetland soils. *Global Biogeochemical Cycles*, *17*(4), 1111. https://doi.org/10.1029/2002GB001917

Chu, H., Baldocchi, D. D., John, R., Wolf, S., & Reichstein, M. (2017). Fluxes all of the time? A primer on the temporal representativeness of FLUXNET. *Journal of Geophysical Research: Biogeosciences*, *122*, 289–307. https://doi.org/10.1002/2016JG003576

Chu, X., Han, G., Xing, Q., Xia, J., Sun, B., Yu, J., & Li, D. (2018). Dual effect of precipitation redistribution on net ecosystem CO_2 exchange of a coastal wetland in the Yellow River delta. *Agricultural and Forest Meteorology*, *249*, 286–296.

Davis, J. L., Currin, C. A., Brien, C. O., Raffenburg, C., & Davis, A. (2015). Living shorelines: Coastal resilience with a blue carbon benefit. *PLOS ONE*, *10*(11), 1–18.

Department for Biogeochemical Integration (2016). *Data processing and plotting utilities of (half-)hourly eddy-covariance measurements*. Jena, Germany: Department for Biogeochemical Integration at MPI-BGC.

Drake, K., Halifax, H., Adamowicz, S. C., & Craft, C. (2015). Carbon sequestration in tidal salt marshes of the northeast United States. *Environmental Management*, *56*(4), 998–1008.

Falge, E., Baldocchi, D., Olson, R., Anthoni, P., Aubinet, M., Bernhofer, C., et al. (2001). Gap filling strategies for defensible annual sums of net ecosystem exchange. *Agricultural and Forest Meteorology*, *107*(1), 43–69.

Finkelstein, P. L., & Sims, P. F. (2001). Sampling error in eddy correlation flux measurements. *Journal of Geophysical Research*, *106*(D4), 3503–3509.

Foken, T., Leuning, R., oncley, S. R., Mauder, M., & Aubinet, M. (2012). Corrections and data quality control. In M. Aubinet, T. Vesala, & D. Papale (Eds.), *Eddy covariance—A practical guide to measurement and data analysis* (pp. 86–132). Dordrecht: Springer.

Forbrich, I., & Giblin, A. E. (2015). Marsh-atmosphere CO_2 exchange in a New England salt marsh. *Journal of Geophysical Research: Biogeosciences*, *120*, 1825–1838. https://doi.org/10.1002/2015JG003044

Gardner, L. R., & Gaines, E. F. (2008). A method for estimating pore water drainage from marsh soils using rainfall and well records. *Estuarine, Coastal and Shelf Science*, *79*(1), 51–58.

Giblin, A. E., & Forbrich, I. (2018a). *PIE LTER high marsh sediment chemistry and activity measurements, Nelson Island Creek marsh*. Rowley, MA: Environmental Data Initiative. https://doi.org/10.6073/pasta/d1d5cbf87602ccf51de30b87b8e46d01

Giblin, A., & Forbrich, I. (2018b). *PIE LTER eddy flux measurements during 2013 from second high marsh site (Spartina patens/short Spartina alterniflora) Tall Tower off Nelson Island Creek*. Rowley, MA: Environmental Data Initiative. https://doi.org/10.6073/pasta/54a15562f2bc25aa91e8c5a6b7d6a8ba

Giblin, A., & Forbrich, I. (2018c). *PIE LTER eddy flux measurements during 2014 from second high marsh site (Spartina patens/short Spartina alterniflora) Tall Tower off Nelson Island Creek*. Rowley, MA: Environmental Data Initiative. https://doi.org/10.6073/pasta/f994f8722ed01c42dedd42aa99492af1

Giblin, A., & Forbrich, I. (2018d). *PIE LTER eddy flux measurements during 2015 from second high marsh site (Spartina patens/short Spartina alterniflora) Tall Tower off Nelson Island Creek*. Rowley, MA: Environmental Data Initiative. https://doi.org/10.6073/pasta/1b635afae834a2327fe627b29df3d96d

Giblin, A., & Forbrich, I. (2018e). *PIE LTER Eddy flux measurements during 2016 from second high marsh site (Spartina patens/short Spartina alterniflora) Tall Tower off Nelson Island Creek*. Rowley, MA: Environmental Data Initiative. https://doi.org/10.6073/pasta/c06c9bb4a599198eba58830060820736

Giblin, A., & Forbrich, I. (2018f). *PIE LTER Eddy flux measurements during 2017 from second high marsh site (Spartina patens/short Spartina alterniflora) Tall Tower off Nelson Island Creek*. Rowley, MA: Environmental Data Initiative. https://doi.org/10.6073/pasta/b718d36c4c0c3c6ef1eea5dbbdc77074

Gross, M. F., Hardisky, M. A., & Klemas, V. (1990). Inter-annual spatial variability in the response of Spartina alterniflora biomass to amount of precipitation. *Journal of Coastal Research*, *6*(4), 949–960.

Hanson, A., Johnson, R., Wigand, C., Oczkowski, A., Davey, E., & Markham, E. (2016). Responses of Spartina alterniflora to multiple stressors: Changing precipitation patterns, accelerated sea level rise, and nutrient enrichment. *Estuaries and Coasts*, *39*(5), 1376–1385.

Helfter, C., Campbell, C., Dinsmore, K. J., Drewer, J., Coyle, M., Anderson, M., et al. (2015). Drivers of long-term variability in CO_2 net ecosystem exchange in a temperate peatland. *Biogeosciences*, *12*(6), 1799–1811.

Hill, T. D., & Anisfeld, S. C. (2015). Coastal wetland response to sea level rise in Connecticut and New York. *Estuarine, Coastal and Shelf Science*, *163*(Part B), 185–193.

Hopkinson, C., Cai, W.-J., & Hu, X. (2012). Carbon sequestration in wetland dominated coastal systems—A global sink of rapidly diminishing magnitude. *Current Opinion in Environmental Sustainability*, *4*(2), 186–194.

Hughes, A. L., Wilson, A. M., & Morris, J. T. (2012). Hydrologic variability in a salt marsh: Assessing the links between drought and acute marsh dieback. *Estuarine, Coastal and Shelf Science*, *111*, 95–106.

Hwang, Y.-H., & Morris, J. T. (1994). Whole-plant gas exchange responses of Spartina alterniflora (Poaceae) to a range of constant and transient salinities. *American Journal of Botany*, *81*(6), 659–665.

Kearney, W. S., Mariotti, G., Deegan, L. A., & Fagherazzi, S. (2017). Stage-discharge relationship in tidal channels. *Limnology and Oceanography: Methods*, *15*(4), 394–407.

Kljun, N., Calanca, P., Rotach, M. W., & Schmid, H. P. (2015). A simple two-dimensional parameterisation for flux footprint prediction (FFP). *Geoscientific Model Development*, *8*(11), 3695–3713.

Kljun, N., Rotach, M., & Schmid, H. (2002). A three-dimensional backward Lagrangian footprint model for a wide range of boundary-layer stratifications. *Boundary-Layer Meteorology*, *103*(2), 205–226.

Krishnaswamy, S., Lal, D., Martin, J., & Meybeck, M. (1971). Geochronology of lake sediments. *Earth and Planetary Science Letters*, *11*(1), 407–414.

Lund, M., Christensen, T. R., Lindroth, A., & Schubert, P. (2012). Effects of drought conditions on the carbon dioxide dynamics in a temperate peatland. *Environmental Research Letters*, *7*(4), 045704.

Mcleod, E., Chmura, G. L., Bouillon, S., Salm, R., Björk, M., Duarte, C. M., et al. (2011). A blueprint for blue carbon: Toward an improved understanding of the role of vegetated coastal habitats in sequestering CO_2. *Frontiers in Ecology and the Environment*, *9*(10), 552–560.

Millette, T. L., Argow, B. A., Marcano, E., Hayward, C., Hopkinson, C. S., & Valentine, V. (2010). Salt marsh geomorphological analyses via integration of multitemporal multispectral remote sensing with lidar and GIS. *Journal of Coastal Research*, *26*(5), 809–816.

Mo, Y., Kearney, M., & Momen, B. (2017). Drought-associated phenological changes of coastal marshes in Louisiana. *Ecosphere*, *8*(5), e01811.

Moore, C. (1986). Frequency response corrections for eddy correlation systems. *Boundary-Layer Meteorology*, *37*(1-2), 17–35.

Morris, J. T. (1984). Effects of oxygen and salinity on ammonium uptake by Spartina alterniflora Loisel. and Spartina patens (Aiton) Muhl. *Journal of Experimental Marine Biology and Ecology*, *78*(1), 87–98.

Morris, J. T. (2000). Effects of sea level anomalies on estuarine processes, *Estuarine science: A synthetic approach to research and practice* (pp. 107–127).

Morris, J. T., & Bowden, W. (1986). A mechanistic, numerical model of sedimentation, mineralization, and decomposition for marsh sediments. *Soil Science Society of America Journal*, *50*, 96–105.
Morris, J. T., & Haskin, B. (1990). A 5-yr record of aerial primary production and stand characteristics of Spartina alterniflora. *Ecology*, *71*(6), 2209–2217.
Morris, J. T., Sundareshwar, P., Nietch, C. T., Kjerfve, B., & Cahoon, D. (2002). Responses of coastal wetlands to rising sea level. *Ecology*, *83*(10), 2869–2877.
Morris, J. T., Sundberg, K., & Hokinson, C. S. (2013). Salt marsh primary production and its responses to relative sea level and nutrients in estuaries at Plum Island, Massachusetts, and North Inlet, South Carolina, USA. *Oceanography*, *26*(3), 78–84.
Morris, J. T., Barber, D. C., Callaway, J. C., Chambers, R., Hagen, S. C., Hopkinson, C. S., et al. (2016). Contributions of organic and inorganic matter to sediment volume and accretion in tidal wetlands at steady state. *Earth's Future*, *4*, 110–121. https://doi.org/10.1002/2015EF000334
Novick, K., Walker, J., Chan, W., Schmidt, A., Sobek, C., & Vose, J. (2013). Eddy covariance measurements with a new fast-response, enclosed-path analyzer: Spectral characteristics and cross-system comparisons. *Agricultural and Forest Meteorology*, *181*(0), 17–32.
O'Connell, J. L., Mishra, D. R., Cotten, D. L., Wang, L., & Alber, M. (2017). The tidal marsh inundation index (TMII): An inundation filter to flag flooded pixels and improve MODIS tidal marsh vegetation time-series analysis. *Remote Sensing of Environment*, *201*(Supplement C), 34–46.
Papale, D., Reichstein, M., Aubinet, M., Canfora, E., Bernhofer, C., Kutsch, W., et al. (2006). Towards a standardized processing of net ecosystem exchange measured with eddy covariance technique: Algorithms and uncertainty estimation. *Biogeosciences*, *3*(4), 571–583.
Peichl, M., Öquist, M., Löfvenius, M. O., Ilstedt, U., Sagerfors, J., Grelle, A., et al. (2014). A 12-year record reveals pre-growing season temperature and water table level threshold effects on the net carbon dioxide exchange in a boreal fen. *Environmental Research Letters*, *9*(5), 055006.
Pelletier, L., Strachan, I. B., Roulet, N. T., Garneau, M., & Wischnewski, K. (2015). Effect of open water pools on ecosystem scale surface-atmosphere carbon dioxide exchange in a boreal peatland. *Biogeochemistry*, *124*(1), 291–304.
Raymond, A. P., & Hopkinson, S. C. (2003). Ecosystem modulation of dissolved carbon age in a temperate marsh-dominated estuary. *Ecosystems*, *6*(7), 694–705.
Redfield, A. (1965). The ontogeny of a New England salt marsh. *Science*, *147*(3653), 50–55.
Reichstein, M., Falge, E., Baldocchi, D., Papale, D., Aubinet, M., Berbigier, P., et al. (2005). On the separation of net ecosystem exchange into assimilation and ecosystem respiration: Review and improved algorithm. *Global Change Biology*, *11*(9), 1424–1439.
Richardson, A. D., & Hollinger, D. Y. (2007). A method to estimate the additional uncertainty in gap-filled NEE resulting from long gaps in the CO_2 flux record. *Agricultural and Forest Meteorology*, *147*(3-4), 199–208.
Troxler, T. G., Gaiser, E., Barr, J., Fuentes, J. D., Jaffe, R., Childers, D. L., et al. (2013). Integrated carbon budget models for the Everglades terrestrial-coastal-oceanic gradient: Current status and needs for inter-site comparisons. *Oceanography*, *26*(3), 98–107.
Vallino, J., Hopkinson, C., & Garritt, R. (2005). Estimating estuarine gross production, community respiration and net ecosystem production: A nonlinear inverse technique. *Ecological Modelling*, *187*(2), 281–296.
Wang, S. R., Di Iorio, D., Cai, W.-J., & Hopkinson, C. S. (2017). Inorganic carbon and oxygen dynamics in a marsh-dominated estuary. *Limnology and Oceanography*, *63*(1), 47–71. https://doi.org/10.1002/lno.10614
Wang, Z. A., Kroeger, K. D., Ganju, N. K., Gonneea, M. E., & Chu, S. N. (2016). Intertidal salt marshes as an important source of inorganic carbon to the coastal ocean. *Limnology and Oceanography*, *61*(5), 1916–1931.
Wieski, K., & Pennings, S. C. (2014). Climate drivers of Spartina alterniflora saltmarsh production in Georgia, USA. *Ecosystems*, *17*(3), 473–484.
Wilson, C. A., Hughes, Z. J., FitzGerald, D. M., Hopkinson, C. S., Valentine, V., & Kolker, A. S. (2014). Saltmarsh pool and tidal creek morphodynamics: Dynamic equilibrium of northern latitude saltmarshes? *Geomorphology*, *213*(0), 99–115.
Wilson, T., & Meyers, T. (2007). Determining vegetation indices from solar and photosynthetically active radiation fluxes. *Agricultural and Forest Meteorology*, *144*(3-4), 160–179.
Zscheischler, J., Fatichi, S., Wolf, S., Blanken, P. D., Bohrer, G., Clark, K., et al. (2016). Short-term favorable weather conditions are an important control of interannual variability in carbon and water fluxes. *Journal of Geophysical Research: Biogeosciences*, *121*, 2186–2198. https://doi.org/10.1002/2016JG003503